Appl Phys B (2009) 96: 423–432
DOI 10.1007/s00340-009-3502-3

Applied Physics B
Lasers and Optics

Linear and nonlinear optical properties of MgO:$LiTaO_3$

I. Dolev · A. Ganany-Padowicz · O. Gayer · A. Arie · J. Mangin · G. Gadret

Received: 16 December 2008 / Published online: 3 April 2009

Abstract We derive new temperature dependent Sellmeier equations for the extra-ordinary and ordinary refractive indices of 0.5% MgO-doped stoichiometric $LiTaO_3$ crystal. The equations are based on quasi phase-matched frequency conversion measurements, as well as on interferometric measurements of the thermal expansion and thermal dispersion. These equations fit experimental data over wide spectral ranges: 0.35–6 μm for the extra-ordinary wave and 0.375–3.75 μm for the ordinary wave, from room temperature up to 200°C. The nonlinear optical measurements set lower-limit values for the d_{33}, d_{22}, and d_{24} elements of the second-order susceptibility tensor $\chi^{(2)}$ of 12.9, 1.54, and 0.46 pm/V, respectively. The interferometric measurements enable one to determine the linear and quadratic expansion coefficients of 1.45762e−5 1/°C, and 2.68608e−8 $(1/°C)^2$, respectively. The Sellmeier equations are in good agreement with previously published data.

PACS 42.65.An · 42.70.Mp · 77.84.Dy

1 Introduction

Periodically poled stoichiometric lithium tantalate (PPSLT) is a widely used crystal in nonlinear optics owing to its wide transparency range (0.27–6 μm), large nonlinear coefficients [1], and high resistance to optical damage [2]. Stoichiometric $LiTaO_3$ (SLT) crystal is now available commercially, and its low coercive field relative to congruent $LiTaO_3$ allows for poling thick samples using the electric field poling technique for quasi phase-matched (QPM) frequency conversion applications [3]. Due to the highest nonlinear susceptibility tensor element, d_{33}, the most commonly used interaction is e-ee, where two extra-ordinary waves induce an extra-ordinary nonlinear polarization. Furthermore, SLT crystal belongs to the trigonal 3m (C_{3v}) crystallographic point group, hence, its second-order susceptibility tensor $\chi^{(2)}$ has several additional non-zero elements. These elements allow for three more types of nonlinear interactions: o-oo (d_{22}, d_{21}, d_{16}), e-oo (d_{31}, d_{32}), and o-eo (d_{24}, d_{15}) [4]. For example, in o-eo interaction, ordinary and extra-ordinary waves generate an ordinary second harmonic. For the e-ee interactions only the extra-ordinary refractive index $n_e(\lambda, T)$ is required, but for the other interactions the ordinary refractive index $n_o(\lambda, T)$ is required as well.

Recently, the ordinary refractive index $n_o(\lambda, T)$ was used in a QPM experiment with another trigonal 3m crystal ($LiNbO_3$) where both the fundamental and the second harmonic (SH) waves were ordinary waves (o-oo, d_{22}) [5]. The application of both ordinary and extra-ordinary indices was proposed in the realization of second-order cascading processes [6] and in quantum information applications where o-eo interactions can be applied for the realization of multipartite continuous-variable entanglement [7]. Knowledge of the refractive-index dispersion equations (Sellmeier equations) of SLT in both the ordinary and extraordinary polarizations is therefore essential with an accuracy of 0.0001.

Sellmeier equations for SLT were obtained in several works. Nakamura et al. [8] and Juvalta et al. [9] obtained

I. Dolev (✉) · A. Ganany-Padowicz · O. Gayer · A. Arie
Department of Physical Electronics, School of Electrical Engineering, Tel Aviv University, Tel-Aviv 69978, Israel
e-mail: idodolev@post.tau.ac.il
Fax: +972-3-6423508

J. Mangin · G. Gadret
Department OMR, Institut Carnot de Bourgogne, UMR-CNRS 5209, 9 Allée Alain Savary, BP 47870 21078 Dijon Cédex, France

Sellmeier equations for both $n_e(\lambda)$ and $n_o(\lambda)$ at room temperature in the spectral range of 0.44–1.05 μm and 275–500 nm, respectively. Abedin et al. [10] derived Sellmeier equations for both $n_e(\lambda, T)$ and $n_o(\lambda, T)$, in the spectral range of 0.4–4 μm and temperature range of 25–300°C. Bruner et al. [11] derived a Sellmeier equation for $n_e(\lambda, T)$, in spectral range of 0.39–4.1 μm and temperature range of 30–200°C. The latter spectral range was further extended to mid-infrared by Kolev et al. [12], both using QPM measurement technique. Although the above mentioned works cover most of the temperature and spectral range for most applications, the data obtained so far are insufficient for design of nonlinear optical devices, specifically those involving both $n_e(\lambda, T)$ and $n_o(\lambda, T)$. For example, Saltiel et al. [13] showed discrepancies between the theoretical equations and experimental measurements.

In this paper we present Sellmeier equations that are applicable for a wide spectral and thermal range. We obtained the Sellmeier equations by measurements of nonlinear interactions with periodically poled crystals involving ordinary polarization, extra-ordinary polarization, and both ordinary and extra-ordinary polarizations. Our measurements also enabled us to obtain absolute and relative value of the $\chi^{(2)}$ tensor elements d_{33}, d_{22}, d_{24}, and d_{32} by nonlinear frequency conversion measurements. In addition, we determine by precise interferometric measurements the thermal expansion and thermal dispersion of the material.

2 Experimental setup

2.1 Thermal expansion and dispersion

The reader is referred to a previous work [14] which describes in detail the principle of the original setup of measurement system that was specifically designed for an accurate determination of the thermo-optic coefficients of nonlinear-optics (NLO) materials. Measurements of linear thermal expansion of millimeter-sized samples are performed using an absolute laser interferometric dilatometer acting as an optical gauge; changes in optical thickness of the same sample are obtained by Fabry–Pérot temperature scanning interferometry [15]. Both setups are operating under vacuum to eliminate the effects of air dispersion. The useful temperature interval extends from −150°C up to +300°C. For a sample of thickness L and refractive index n, the linear thermal expansion and normalized thermo-optic coefficient (NTOC) are defined by $\alpha = d[\ln(L)])/dT$ and $\beta = d[\ln(n)]/dT$, respectively. Defining the coefficient γ for normalized changes in optical thickness, that is $\gamma = d[\ln(Ln)]/dT$, the NTOC is obtained from the straightforward relationship $\beta = \gamma - \alpha$. For a given wavelength λ,

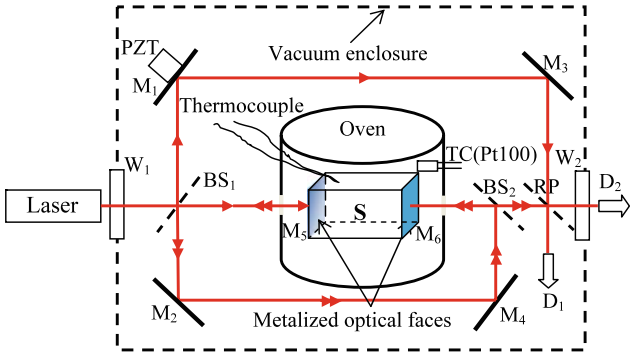

Fig. 1 Absolute interferometric dilatometer used for the determination of thermal expansion coefficients of SLT [14]

a phase shift of 2π (i.e. fringe spacing), induced by a variation of temperature ΔT, corresponds to a change in length (or optical thickness) of $\lambda/2$.

The modified Mach–Zehnder interferometric setup used for dilatation measurements is depicted in Fig. 1. Two silica windows W_1 and W_2 allow for entering and leaving of light from the vacuum enclosure. The beam of a frequency stabilized He-Ne laser is divided into two paths by the beam splitter BS_1. The plane and parallel optical end faces of a parallelepipedic-shaped sample S are gold metalized and act as mirrors M_5 and M_6 in the sample arm. After reflection on the front face M_5, the beam is sent by successive reflections on BS_1, M_2, M_4, and beam splitter BS_2 to the back surface M_6 of the sample. The reflected beam from the sample overlaps the one of the reference arm (path BS_1, M_1, M_3 and RP) at the recombination plate RP to give a fringe pattern, which is recorded by photo-detector D_1. Detection D_2, external to the enclosure, allows also for convenient observation of the fringe pattern on a screen and verification of its stability. Best accuracy of measurements is achieved by inserting a piezo-transducer PZT on mirror M_1 that allows for phase modulation and subsequent phase detection of the fringe shift induced by applying a linear ramp of temperature to the sample through temperature control TC (Pt 100 thermistance) of the oven.

Normalized changes in optical thickness are obtained by removing metallization M_5 and M_6. The same sample S is now mounted in a specific vacuum cell which reproduces identical thermal working conditions as those used in the dilatometer. Appropriate translation and rotation stages enable accurate orientation of the dielectric frame of the sample with respect to the polarization direction of the incident beam. A Fabry–Pérot interference pattern is generated by multiple reflections of a laser beam on the optical end faces; the fringe shift induced by applying a linear ramp of temperature to the sample is observed by reflection and continuously recorded on photo-detector D_1 after being reflected by the semi reflecting plate BS, as shown in Fig. 2. An analyzer crossed with respect to the direction of the front polar-

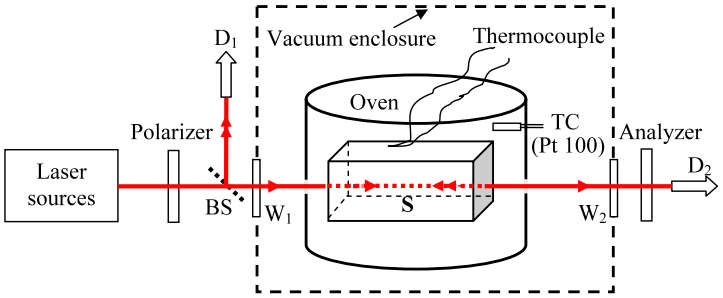

Fig. 2 Experimental setup used for Fabry–Pérot temperature scanning interferometry at several laser wavelengths [15]

izer allows for permanent control of the spatial stability of the sample all along heating runs, by recording on detector D_2 the intensity of the transmitted beam, which is imaged outside the vacuum cell. BaF_2 windows W_1 and W_2 enable convenient switching of laser sources from the UV-Vis up to the IR spectral range.

2.2 Sellmeier equations

The SLT crystals were grown by the double-crucible Czochraski method [16], at Oxide Co. and doped with 0.5% mol MgO. The periodic structured pattern of photoresist was contact printed on the C+ face of the wafer from a lithographic mask and uniformly coated by a metallic layer. The electrical poling was achieved by applying pulses to the polar crystal surfaces using our standard electric field poling technique [17]. The total switching charge was 45 μC/cm^2. After poling, photoresist and metallic coatings were removed and the domain structure was revealed by HF etching. We used several gratings with periods ranging from 7.72 μm to 29.5 μm and with a duty cycle of 50%.

Two types of nonlinear interactions were measured: second harmonic generation (SHG), and difference frequency generation (DFG) obtained by an optical parametric oscillator (OPO) [18]. Briefly, in the SHG setup four types of fundamental beam sources were used: (1) tunable 0.7–0.9 μm Ti:sapphire laser (Tsunami, Spectra-Physics Lasers), (2) Nd:YAG 1.0645 μm laser (Laser Compact model LCS-DTL-122QT), (3) homemade tunable OPO system (1.5–4.1 μm), and (4) tunable cw diode laser (ANDO AQ4321D, 1.52–1.62 μm), with an EDFA to amplify the laser output. In each measurement the fundamental light polarization was controlled, and appropriate detectors and polarizers were used for the output SH. The PPSLT crystals were placed in the center of the beam waist in order to obtain maximum SH efficiency. The PPSLT crystals were staged in a temperature controlled oven with a temperature range of 25°C to 200°C.

A second experimental setup is based on down conversion in a PPSLT OPO. The OPO is pumped by Q-switched Nd:YLF 1.0475 μm laser (Lightwave Electronics model 110) generating signal in the range of 1.4–1.6 μm and idler in the range of 3.3–4.1 μm. In order to obtain the desired signal and idler wavelengths, the PPSLT crystal was staged in a temperature controlled oven with a temperature range of 25°C to 200°C. Only extra-ordinary interactions were efficient enough to surpass the OPO threshold condition.

The SHG and OPO nonlinear interactions involve two or three waves mixing and must fulfill two basics conditions: energy conservation and momentum conservation. The energy conservation of the participating wavelengths requires $\omega_i = \omega_p - \omega_s$ for the OPO interactions and $\omega_s = 2\omega_p$ for SHG, where ω_p is the pump frequency which is down-converted into signal and idler frequencies: ω_s and ω_i, respectively. When a periodically poled crystal is involved in a collinear quasi phase-matching interaction, the momentum conservation or phase-matching condition requires satisfaction of (1) in the case of OPO:

$$\frac{\omega_p \cdot n(\omega_p, T)}{c} - \frac{\omega_s \cdot n(\omega_s, T)}{c} - \frac{\omega_i \cdot n(\omega_i, T)}{c} - \frac{2\pi}{\Lambda(T)} = \Delta k_{opt}, \tag{1}$$

where c is the speed of light. In the case of SHG equation (2) is required:

$$\frac{2\omega \cdot n(2\omega, T)}{c} - \frac{2 \cdot \omega \cdot n(\omega, T)}{c} - \frac{2\pi}{\Lambda(T)} = \Delta k_{opt} \tag{2}$$

where $n(\omega, T)$ represents $n_e(\omega, T)$ or $n_o(\omega, T)$, depending on the specific wave polarization, ω is the fundamental wave frequency, Δk_{opt} is the optimal phase mismatch that generally depends on beam focusing [19] (and equals to zero in the case of plane wave), and $\Lambda(T)$ is the actual crystal poling period, taking into account the thermal expansion:

$$\Lambda(T) = \Lambda(T_0) \exp\left[a(T - T_0) + \frac{1}{2} b\left(T^2 - T_0^2\right)\right]. \tag{3}$$

Since (1) and (2) involve terms of two or three different wavelengths, we used a numerical method to calculate the refractive indices. For each polarization we assumed Sellmeier equations based on the representation used by Jundt

for undoped congruent $LiNbO_3$ [20], with an extension of temperature dependence in both poles:

$$n^2 = a_1 + b_1 f + \frac{a_2 + b_2 f}{\lambda^2 - (a_3 + b_3 f)^2} + \frac{a_4 + b_4 f}{\lambda^2 - (a_5 + b_5 f)^2} - a_6 \lambda^2. \quad (4)$$

Parameter a_6 represents the phonon absorptions in the far-IR. The parameters a_3 and a_5 account for poles in the UV and IR wavelengths, with the weights a_2 and a_4, respectively. Parameter a_1 represents the contributions to the refractive index from plasmons in the far UV [21]. The $b_i f$ parameters represent thermal effects, where f is expressed in terms of a quadratic dependence of the absolute temperature T in Celsius degrees, thus:

$$f = (T - 24.5°\mathrm{C})(T + 24.5°\mathrm{C} + 2 \cdot 273.16). \quad (5)$$

It is interesting to note that previous Sellmeier equations had a different number of poles: Nakamura et al. [8] and Abedin et al. [10] used a single pole in the UV whereas Bruner et al. [11] and Kolev et al. [12] used two poles in the UV and a third pole in the mid-IR. We have found that our form of equation, with only two poles, is sufficient to fit the experimental results with very good accuracy. We used least-square optimization to determine a_i and b_i parameters for the Sellmeier equation (4) that minimized the differences between experimental and calculated values of phase mismatch Δk's, given by (1) and (2). We also gave some weight to data from previously published works, in the spectral and temperature ranges when such data were available.

2.3 Second-order susceptibility tensor elements

The tunable cw diode laser (ANDO AQ4321D) setup was also used to determine the d_{ij} second-order susceptibility tensor elements of SLT. In accordance with the analysis given by Boyd and Kleinman [19] we used the following equation:

$$P_{2\omega} = \frac{2\omega^3 d_{\mathrm{eff}}^2}{\pi n_\omega n_{2\omega} \varepsilon_0 c^4} h_{\mathrm{BK}}(\xi, \sigma) \cdot l \cdot P_\omega^2, \quad (6)$$

where ω and 2ω are the fundamental and SH angular frequencies, respectively, ξ and σ being the respective focusing and phase mismatch parameters; $h_{\mathrm{BK}}(\xi, \sigma)$ is the Boyd–Kleinman efficiency parameter, ε_0 is the vacuum permittivity and d_{eff} the effective nonlinear coefficient involved in the considered QPM process.

3 Results

3.1 Thermal dispersion and expansion coefficients

Absolute interferometric measurements of thermal expansion and normalized thermo-optic coefficients of SLT were performed from −30°C up to 80°C on a parallelepipedic shaped sample with dimensions $4 \times 8 \times 2.5$ mm^3 along the principal X, Y, and Z axes, respectively. The Y-oriented optical end faces were plane and parallel to better than $10''$ of an arc; such geometry enables dilatation measurements only along the direction normal to the polar axis Z (i.e. $\alpha_x = \alpha_y \equiv \alpha_\perp$), while NTOC can be obtained for both ordinary and extraordinary polarization.

Results of linear thermal expansion measurements are depicted in Fig. 3. Over the explored temperature interval it is found that experimental data are well fitted to the linear expansion $\alpha_\perp = 1.45762 \times 10^{-5} + 2.68608 \times 10^{-8} T$, where T is the temperature in Celsius degrees. Figure 4 gives a comparison of the relative thermal expansion $\Delta L/L$ versus temperature between stoichiometric and congruent lithium

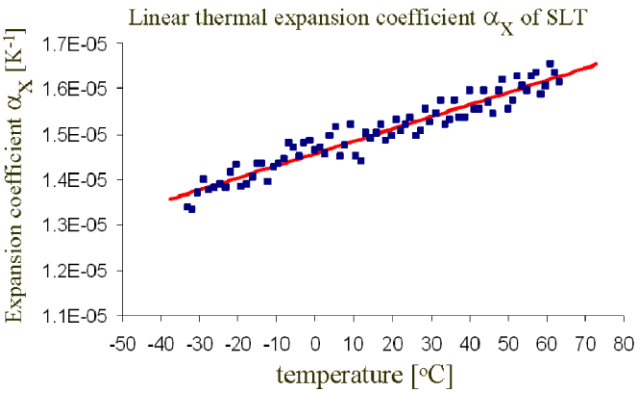

Fig. 3 Principal linear thermal expansion in the (X, Y) plane of SLT from −30°C to 80°C; *blue squares*: measurements, *solid curve* (*red*): linear fit. The deviation of experimental data from the curve fit does not exceed 4×10^{-7} K^{-1}

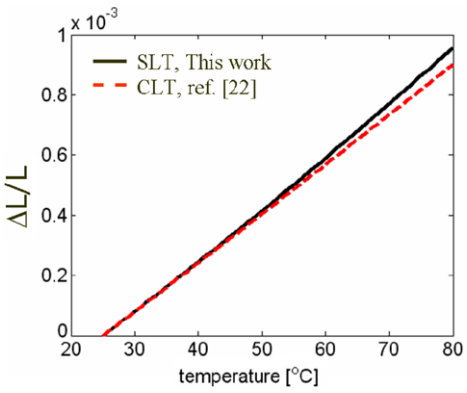

Fig. 4 Comparison of the relative thermal expansion $\Delta L/L$ of stoichiometric and congruent lithium tantalate along the principal axes in the (X, Y) plane

Table 1 Parameters for linear fit of normalized thermo-optic coefficients of SLT, according to the following expansion: $\beta = a_0 + a_1 T$

λ (μm)	$\beta_o = dn_o/n_o\,dT$		$\beta_e = dn_e/n_e\,dT$	
	$a_0 \times 10^6$	$a_1 \times 10^8$	$a_0 \times 10^5$	$a_1 \times 10^8$
0.4545	4.8833	3.3059	2.5658	9.1092
0.4880	4.1763	2.8403	2.4569	8.5596
0.4965	3.9368	2.7386	2.4195	8.4462
0.514	3.5629	2.4884	2.3506	8.3996
0.6328	1.9042	1.7271	2.0792	7.3069
1.0642	0.5586	0.92168	1.8017	6.1500
3.390	0.3329	1.4888	1.4945	3.8973

tantalate [22], the last one being actually used in [11] for a purpose similar to the present one. The difference between both curves reaches 6% at 80°C.

Normalized thermo-optic coefficients were determined at seven wavelengths: measurements of changes in optical thickness were performed at 0.4545, 0.4880, 0.4965 and 0.5140 μm with a tunable argon ion laser, at 0.6328 and 3.39 μm with He-Ne lasers, and at 1.0642 μm with a cw Nd:YAG laser. The NTOC's β_o and β_e were derived from these measurements at each wavelength and for both ordinary and extra-ordinary polarizations, taking into account the thermal expansion of the sample as described above. The results are summarized in Table 1, which gives the parameters of the linear fits of NTOC's, which were found well suited to represent their evolution over the −30°C–80°C temperature interval.

The thermal expansion and dispersion coefficients are crucial for the design of temperature-tuned nonlinear devices, and they were also used for the derivation of the crystal's Sellmeier equations.

3.2 Sellmeier equations

The SHG measurements were conducted over a wide range of temperatures, on going from room temperature up to 200°C for each PPSLT crystal and for both ordinary and extra-ordinary polarizations. For the tunable sources (Ti:sapphire laser, ANDO diode laser and the homemade OPO), the laser wavelength was tuned to a value in which maximum SH signal was obtained at each temperature. When non-tunable laser (YAG) was used the temperature was tuned to a value in which maximum SH signal was obtained, assuming this wavelength satisfying the phase-matching conditions as defined in (1) and (2). The SHG measurements were further extended to high-order SHG interactions in which the effective crystal period in (2) is divided by the corresponding QPM order m,

$$\Lambda_{\text{effective}} = \frac{\Lambda}{m}. \tag{7}$$

The SH experimental data are summarized in Table 2.

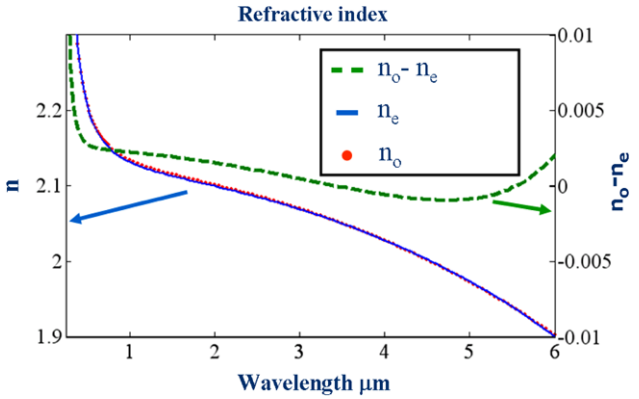

Fig. 5 Refractive indices for 0.5% MgO-doped SLT at 150°C. Left ordinate, n_e (*solid line*) and n_o (*dots*) refractive indices. Right ordinate (*dashed line*), delta between n_o and n_e

The OPO measurements (e-ee) were performed using SLT crystals with periods of 28.5 μm and 29.5 μm. The OPO signal and the idler spectra were measured for both periods in the temperature range of 25–200°C.

OPO and SHG measurements for the extra-ordinary waves and SHG measurements for the ordinary waves were used for calculating the Sellmeier parameters of 0.5% MgO-doped SLT crystal. The calculated parameters for the new Sellmeier equations are presented in Table 3. The refractive indices curves vs. wavelength at 150°C, are shown in Fig. 5. The interacting wavelengths extend from the UV up to the mid-IR spectral range. The OPO idler and signal spectra are shown in Fig. 6, along with the theoretical spectra calculated from our Sellmeier equations. The SHG measurements of the e-oo and o-eo interactions, involving both ordinary and extra-ordinary refractive indices, cross validate the new parameters.

3.3 Second-order susceptibility tensor elements

We measured the SH power versus pump wavelength at fixed temperatures, the SH power versus crystal temperature at chosen pump wavelength, and the SH power versus pump power for all interactions (e-ee, o-oo, o-eo, e-oo) in 21.2 μm poling period SLT using the tunable cw diode laser (ANDO AQ4321D) setup. The results for the o-oo interactions with the theoretical curves are shown in Fig. 7. We deduced the external conversion efficiency coefficients of: 0.229% W^{-1}, 3.3e−3% W^{-1}, 4.48e−4% W^{-1}, and 4.38e−4% W^{-1}, for the e-ee, o-oo, o-eo, and e-oo interactions, respectively. Taking into account the poling length (16 mm) and the Fresnel reflection losses of the fundamental wave and the SH wave, the normalized internal conversion efficiencies obtained are 24.89% $W^{-1}m^{-1}$, 0.35% $W^{-1}m^{-1}$, 0.032% $W^{-1}m^{-1}$, and 0.031% $W^{-1}m^{-1}$ for the e-ee, o-oo, o-eo, and e-oo interactions, respectively. By using (6) of Boyd and Kleinman [19], we have derived a lower-limit value of $d_{33} = 12.9$, $d_{22} =$

Table 2 Summary of the SHG experiments. The measurements were conducted from room temperature to 200°C

SLT period [μm]	Process	Fundamental wavelength [μm]	SH wavelength [μm]	Phase-matching temperature [°C]	Order (m)
7.72	e-ee, o-oo	1.064	0.532	o-oo: 206, e-ee: 160	1
7.72	e-ee	0.866–0.847	0.423–0.433	80 for 0.851 μm	2
7.72	e-ee, o-oo	0.756–0.772	0.378–0.386	0.760 μm: 70 for o-oo, 90 for e-ee	3
7.72	e-ee	0.699–0.716	0.349–0.358	60 for 0.702 μm	4
19.8	o-eo, e-oo	1.530–1.552	0.765–0.776	o-eo: 25.3 for 1.5303 μm, e-oo: 105 for 1.5403 μm	1
20.5	e-ee, o-oo o-eo, e-oo	1.526–1.556	0.763–0.778	e-ee: 80 for 1.5379 μm, o-oo: 80 for 1.5404 μm, o-eo: 60 for 1.5432 μm, e-oo: 80 for 1.5402 μm	1
21.2	e-ee, o-oo o-eo, e-oo	1.551–1.578	0.775–0.789	e-ee: 80 for 1.5603 μm, o-oo: 80 for 1.5661 μm, o-eo: 100 for 1.551 μm, e-oo: 80 for 1.5642 μm	1
21.8	e-ee	1.574–1.578	0.787–0.789	40 for 1.574 μm	1
28.5	e-ee, o-oo	3.750–3.879	1.875–1.940	e-ee: 100 for 3.848 μm, o-oo: 180 for 3.755 μm	1
28.5	e-ee	0.862–0.878	0.431–0.439	140 for 0.869 μm	7
28.5	e-ee	0.757–0.773	0.378–0.386	100 for 0.762 μm	11

Table 3 Calculated Sellmeier coefficients for 0.5% MgO-doped stoichiometric $LiTaO_3$ (SLT); λ is given in microns

Parameter	0.5% MgO-doped SLT	
	n_e	n_o
a_1	4.5615	4.5082
a_2	0.08488	0.084888
a_3	0.1927	0.19552
a_4	5.5832	1.1570
a_5	8.3067	8.2517
a_6	0.021696	0.0237
b_1	4.782e−7	2.0704e−8
b_2	3.0913e−8	1.4449e−8
b_3	2.7326e−8	1.5978e−8
b_4	1.4837e−5	4.7686e−6
b_5	1.3647e−7	1.1127e−5

1.54, $d_{24} = 0.46$, and $d_{32} = 0.45$ pm/V for each tensor element. In fact, owing to Kleinman symmetry [4] we expect that $d_{24} = d_{32}$, hence the small difference is probably owing to experimental inaccuracy.

4 Discussion

Deduced from our new Sellmeier equations, Figs. 8 and 9 display the dispersion of the normalized thermo-optic coefficient from around 0.4 μm up to 4 μm for the extra-ordinary and ordinary polarization, respectively. An excellent agreement with absolute interferometric measurements can be observed; this is not the case for previously published equations that we have drawn on the same graphs for comparison: all of them exhibit significant deviation from our experimental data, except to some extent data due to Abedin et al. [10] in a representation for the ordinary index at short wavelengths.

We compared our refractive indices at 80°C with previously published works (Fig. 10). The $n_e(\lambda, T)$ values of the extra ordinary index obtained from our Sellmeier equation differ by ∼0.002 from those of Bruner et al. [11] and Kolev et al. [12]. At wavelengths 0.35–6 μm the deviation is estimated to lie around ∼0.006 in the case of the ordinary index when compared to the work of Abedin et al. [10]. It is interesting to notice that the SLT crystal becomes negative to

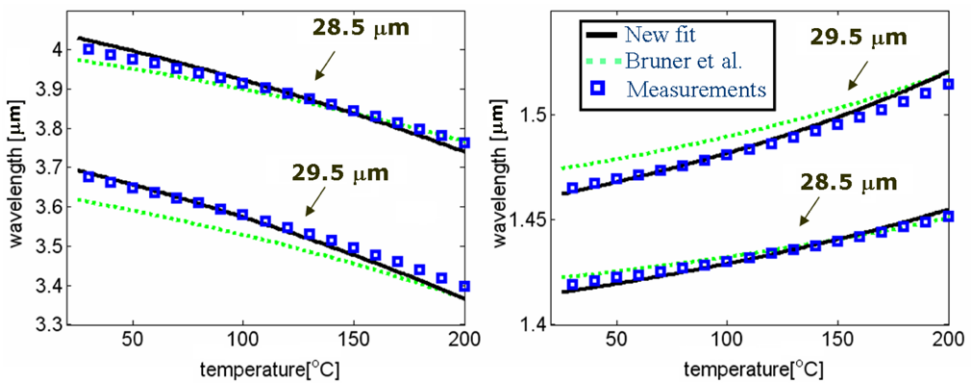

Fig. 6 OPO signal and idler wavelength spectra vs. temperature for PPSLT. The results are compared with the new theoretical Sellmeier equation and with Bruner et al. [11]

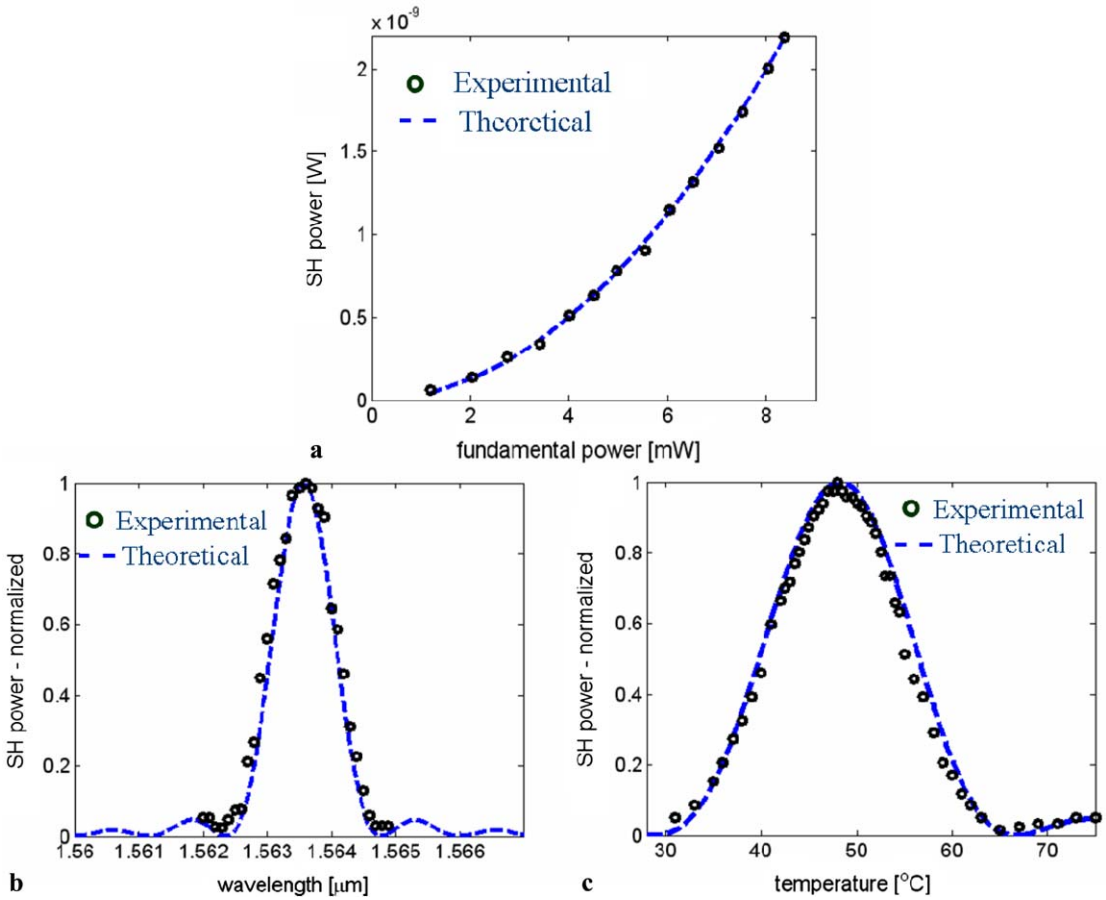

Fig. 7 First order o-oo interactions in 21.2 μm poling period crystal. All measurements show excellent agreement with theoretical curves. (**a**) SH power versus pump power at fixed wavelength and temperature. (**b**) SH power versus pump wavelength at 50°C. (**c**) SH power versus crystal temperature, pump wavelength 1563.4 nm

positive uniaxial between 3.45–5.55 μm at room temperature.

A comparison of different $n_e(\lambda, T)$ equations with our SHG measurements is shown in Fig. 11. The phase-matched wavelengths of a 28.5 μm crystal period are given at each chosen temperature and compared to theoretical curves calculated from our equation and the equations of Abedin et al. [10], Juvalta et al. [9], Nakamura et al. [8], and Bruner et al. [11]. The new Sellmeier equation shows better agreement with our SHG results relative to the previously published equations. Although the equation of Bruner et al. [11] appears in good agreement with the 28.5 μm crystal SHG, it showed however a noticeable deviation from OPO tuning curve measurements. Our equation fits better to the OPO tuning curve measurements, as can be verified in Fig. 7.

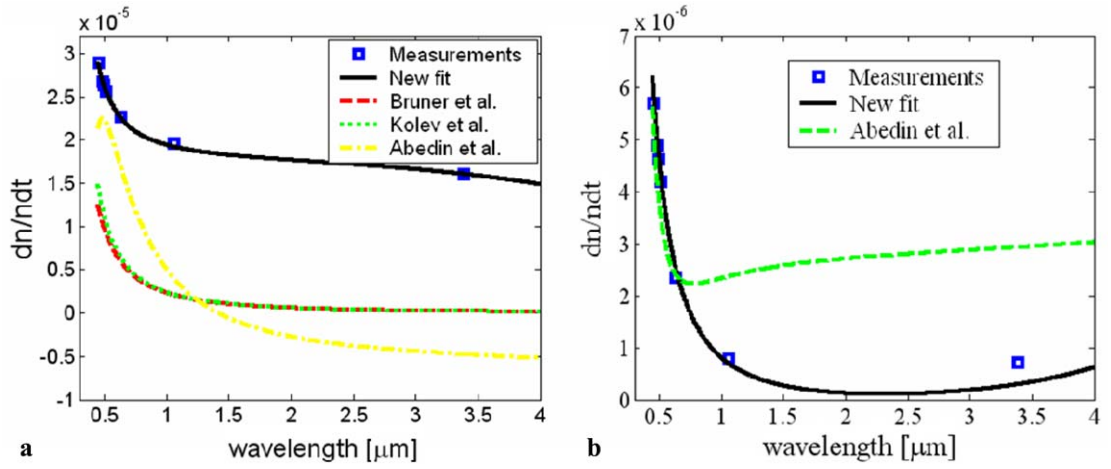

Fig. 8 Room temperature $dn/n\,dt$ vs. wavelength. (**a**) Our experimental n_e data, the theoretical curves of the new Sellmeier equation, Abedin et al. [10], Kolev et al. [12], and Bruner et al. [11] are presented. (**b**) Our experimental n_o data, the theoretical curves of the new Sellmeier equation, and Abedin et al. [10]

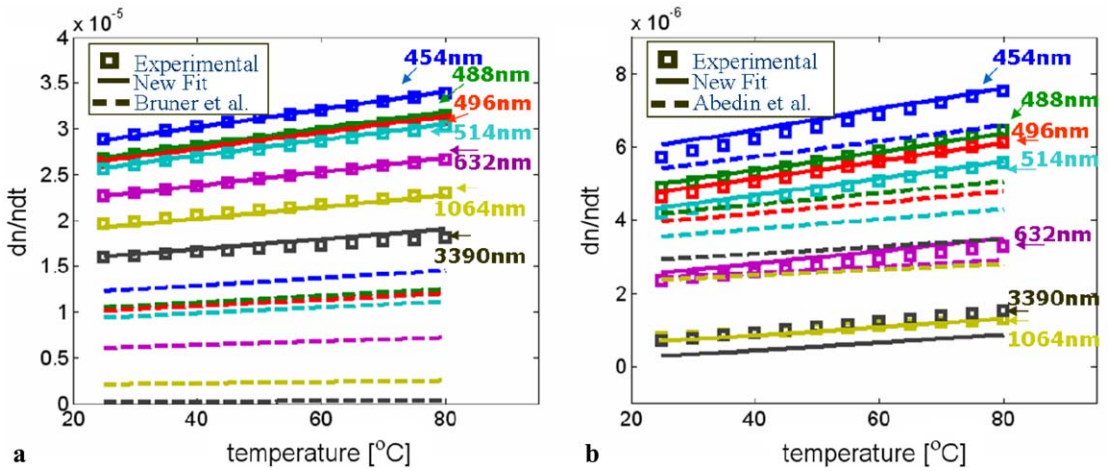

Fig. 9 $dn/n\,dt$ vs. temperature. (**a**) Our experimental n_e data, the theoretical curves of the new Sellmeier equation, and Bruner et al. [11]. (**b**) Our experimental n_o data, the theoretical curves of the new Sellmeier equation, and Abedin et al. [10]

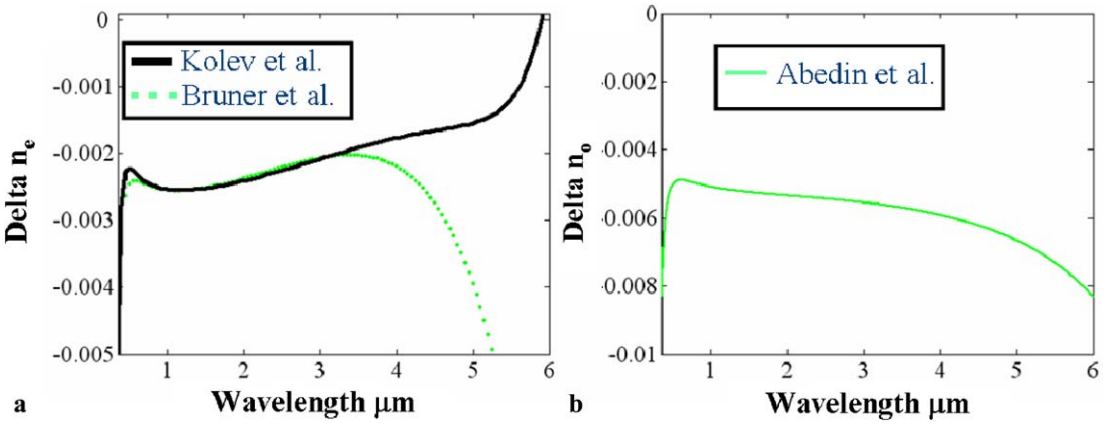

Fig. 10 Comparison between the refractive indices obtained at 80°C and the refractive indices in literature. The ordinate represents the delta between our calculated refractive index and previously published data. For extra-ordinary index (**a**): *dashed line*, Bruner et al. [11]; *solid line*, Kolev et al. [12]. For ordinary refractive index (**b**): Abedin et al. [10]

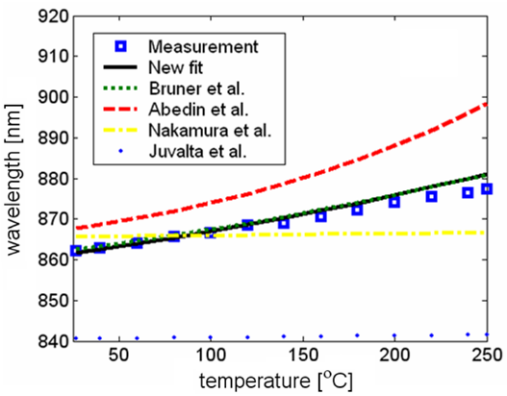

Fig. 11 Seventh-order e-ee QPM interactions in 28.5 μm period PPSLT as function of wavelength and temperature. Our experimental data, the theoretical curves of the new Sellmeier equation, and the equations of Abedin et al. [10], Juvalta et al. [9], Nakamura et al. [8], and Bruner et al. [11] are presented

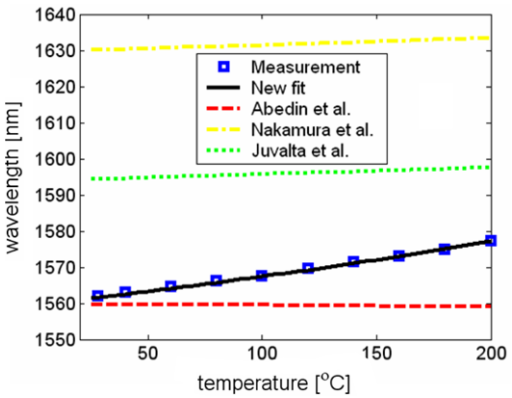

Fig. 12 First order o-oo QPM interactions in 21.2 μm period PPSLT as a function of wavelength and temperature. Our experimental data, the theoretical curves of the new Sellmeier equation, and the equations of Abedin et al. [10], Juvalta et al. [9], and Nakamura et al. [8] are presented

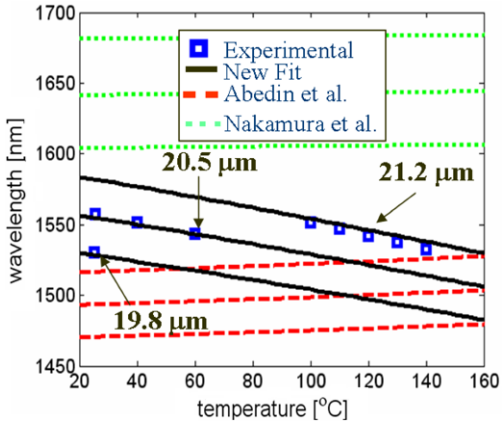

Fig. 13 First order o-eo QPM interactions in 19.8 μm, 20.5 μm, and 21.2 μm periods PPSLT as a function of wavelength and temperature. Our experimental data, the theoretical curves of the new Sellmeier equation, and the equations of Abedin et al. [10] and Nakamura et al. [8] are presented

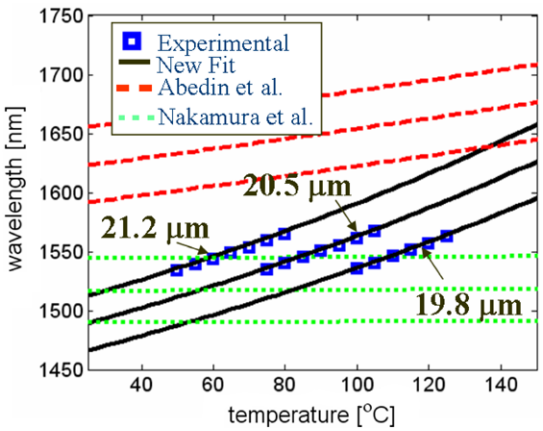

Fig. 14 First order e-oo QPM interactions in PPSLT as a function of wavelength and temperature. Our experimental data, the theoretical curves of the new Sellmeier equation, and the equations of Abedin et al. [10], and Nakamura et al. [8] are presented

We compared also the new $n_e(\lambda, T)$ equation to previously published experimental results that include OPO spectra in the near-IR and mid-IR [3, 12, 23]. In all cases the new equation fits to the experimental results with high accuracy.

A comparison of different $n_o(\lambda, T)$ equations with our SHG measurements is shown in Fig. 12. The phase-matched wavelengths at each temperature are given for a crystal period of 21.2 μm, and compared with theoretical curves calculated according to the new equation and the equations of Abedin et al. [10], Nakamura et al. [8], and Juvalta et al. [9]. The new equation shows excellent agreement with our SHG results. On the other hand, the previously published equations show significant deviation from our experimental data.

Equations (1) and (2) involve terms of two or three different refractive indices. While most measured interactions involve either ordinary or extra-ordinary refractive indices, the o-eo and e-oo SHG measurements contain both and therefore cross validate the Sellmeier equations. The o-eo and e-oo measurements are presented in Figs. 13 and 14, respectively. The new equations are in excellent agreement with our SHG results. Equations obtained from previously published works deviate significantly from our experimental observations. It may be noted also that despite that NTOC's measurements were obtained only in the restricted −30°C–+80°C temperature range, it appears from high temperature SHG measurements that their dispersion should also be valid at least up to 200°C.

The measured nonlinear coefficients ($d_{33} = 12.9$, $d_{22} = 1.54$, and $d_{24} = 0.46$ pm/V) are lower than the previously published values of: $d_{33} = 16$, $d_{22} = 1.7$, and $d_{24} = 1$ pm/V [24] since in the latter ones the PPSLT is assumed to have a perfect 50% duty cycle throughout the entire poling length

and due to inaccuracies in experimental conditions. Nevertheless, the relative values of the nonlinear coefficients (e.g. with respect to d_{33}) should be accurate since all measurements were performed in the same conditions, hence they do not depend on any absolute calibration. The d_{ij} vs. d_{33} ratios are 0.12 (d_{22}), and 0.035 (d_{24}), whereas [24] predicts ratios of 0.11, and 0.062, respectively. The efficiency of the QPM interaction is proportional to the square of the nonlinear coefficient (equation (6)) and therefore the ratio values suggest that the e-ee process is more efficient by almost 2 orders of magnitude when compared to o-oo process and by 3 orders of magnitude when compared to e-oo and o-eo interactions.

The full width at half maximum of SH power versus temperature of the 21.2 μm poling period of the crystals for e-ee, o-oo, e-oo, and o-eo interactions are 7°C, 14°C, 1.2°C, and 2°C, respectively. These results suggest that the interactions involving both ordinary and extra-ordinary refractive indices have a much stronger temperature dependence compared to the e-ee and o-oo interactions.

5 Summary and conclusions

In this work we present wavelength and temperature dependent refractive-index equations for 0.5% MgO-doped stoichiometric $LiTaO_3$ crystal. We obtained new Sellmeier coefficients from quasi phase-matched frequency conversion measurements, as well as thermal expansion and thermal dispersion coefficients using interferometric measurements. Our new Sellmeier equation for the extra-ordinary index is in good agreement with previously published data as well as with our own experimental results. We suggest a new ordinary refractive-index equation, which deviates significantly from all previous equations and is in good agreement with our experimental results. The new equations were cross validated with measurements of o-eo and e-oo interactions, involving both ordinary and extra-ordinary refractive indices. The $n_e(\lambda, T)$ equations for 0.5% MgO-doped SLT is valid for 0.35–6 μm spectral range and 25–200°C temperature range. Due to insufficient data we were not able to further test the validity of the $n_o(\lambda, T)$ equation in the entire spectral and thermal ranges. We therefore consider our ordinary refractive-index Sellmeier equation to be reliable in the wavelength range of 0.375–3.75 μm and temperature range of 25–200°C. We also provided a lower-limit value for the d_{33}, d_{22}, and d_{24} elements of the second-order susceptibility tensor $\chi^{(2)}$ and deduced their ratios. We showed that the o-eo and e-oo interactions are strongly dependent on the crystal temperature as compared to o-oo and e-ee interactions. The derived coefficients for the linear and nonlinear properties should be useful for the design of nonlinear optical devices based on any second-order interaction in MgO-doped SLT.

Acknowledgements The authors thank Prof. Israel Gannot for the use of the Ti:sapphire laser and Dr. Alex Skliar form Raicol crystals for providing SLT samples. This work was supported by the Israeli Ministry of Science, Culture and Sport.

References

1. S.N. Zhu, Y.Y. Zhu, H.F. Wang, Z.Y. Zhang, N.B. Ming, W.Z. Shen, Y. Chang, X.C. Shen, J. Phys. D Appl. Phys. **28**, 2389–2391 (1995)
2. G.L. Tangonan, M.K. Barnoski, J.F. Lotspeich, A. Lee, Appl. Phys. Lett. **30**, 238–239 (1977)
3. T. Hatanaka, K. Nakamura, T. Taniuchi, H. Ito, Y. Furukawa, K. Kitamura, Opt. Lett. **25**, 651–653 (2000)
4. R.W. Boyd, *Nonlinear Optics* (Academic Press, San Diego, 2003)
5. A. Ganany, A. Arie, S.M. Saltiel, Appl. Phys. B-Lasers Opt. **85**, 97–100 (2006)
6. S. Saltiel, Y. Deyanova, Opt. Lett. **24**, 1296–1298 (1999)
7. R.C. Pooser, O. Pfister, Opt. Lett. **30**, 2635–2637 (2005)
8. M. Nakamura, S. Higuchi, S. Takekawa, K. Terabe, Y. Furukawa, K. Kitamura, Jpn. J. Appl. Phys. **41**(2), L465–L467 (2002)
9. F. Juvalta, M. Jazbinsek, P. Gunter, K. Kitamura, J. Opt. Soc. Am. B **23**, 276–281 (2006)
10. K.S. Abedin, H. Ito, J. Appl. Phys. **80**, 6561–6563 (1996)
11. A. Bruner, D. Eger, M.B. Oron, P. Blau, M. Katz, S. Ruschin, Opt. Lett. **28**, 194–196 (2003)
12. V.Z. Kolev, M.W. Duering, B. Luther-Davies, Opt. Lett. **31**, 2033–2035 (2006)
13. S.M. Saltiel, D.N. Neshev, R. Fischer, W. Krolikowski, A. Arie, Y.S. Kivshar, Phys. Rev. Lett. **100** (2008)
14. J. Mangin, P. Strimer, L. Lahloukassi, Meas. Sci. Technol. **4**, 826–834 (1993)
15. J. Mangin, G. Gadret, S. Fossier, P. Strimer, IEEE J. Quantum Electron. **41**, 1002–1006 (2005)
16. Y. Furukawa, K. Kitamura, E. Suzuki, K. Niwa, J. Cryst. Growth **197**, 889–895 (1999)
17. A. Bruner, D. Eger, S. Ruschin, J. Appl. Phys. **96**, 7445–7449 (2004)
18. I. Dolev, A.G. Padowicz, O. Gayer, A. Arie, IEEE 308–312 (2008)
19. G.D. Boyd, D.A. Kleinman, J. Appl. Phys. **39**, 3597 (1968)
20. D.H. Jundt, Opt. Lett. **22**, 1553–1555 (1997)
21. U. Schlarb, K. Betzler, Phys. Rev. B **50**, 751–757 (1994)
22. Y.S. Kim, R.T. Smith, J. Appl. Phys. **40**, 4637–4641 (1969)
23. N.E. Yu, S. Kurimura, Y. Nomura, M. Nakamura, K. Kitamura, J. Sakuma, Y. Otani, A. Shiratori, Appl. Phys. Lett. **84**, 1662–1664 (2004)
24. W. Martienssen, H. Warlimont, *Springer Handbook of Condensed Matter and Materials Data* (Springer, Berlin, 2005)